Electrochimica Acta 212 (2016) 141–146

Contents lists available at ScienceDirect

Electrochimica Acta

journal homepage: www.elsevier.com/locate/electacta

A Facile 3D Binding Approach for High Si Loading Anodes

Yitian Bie[a], Jun Yang[a,*], Wei Lu[b], Zhihong Lei[a], Yanna Nuli[a], Jiulin Wang[a]

[a] School of Chemistry and Chemical Engineering, Shanghai Jiao Tong University, Shanghai, 200240, China
[b] Department of Chemical Engineering, University of Michigan, Ann Arbor, MI 48109, USA

ARTICLE INFO

Article history:
Received 7 April 2016
Received in revised form 10 June 2016
Accepted 28 June 2016
Available online 29 June 2016

Keywords:
Silicon
Binder
Silane coupling agent
Crosslinking
Lithium-ion battery

ABSTRACT

Silicon is regarded as one of the most promising anode materials for Li-ion batteries owing to its high theoretical capacity (4200 mA h g^{-1}, $Li_{22}Si_5$), but the short cycle life mainly caused by the dramatic volume effect has hindered its practical application. To address this major issue, we report here an effective and scalable approach to fabricate a novel Si electrode via the addition of silane coupling agent, which not only connects silicon and polyacrylic acid (PAA) covalently but also crosslinks PAA, thus forming an entire 3D binding network. The dual functions of 3-amino-propyltriethoxysilane (APTES) in an electrode with 80% Si nanoparticles greatly improves the structural stability during the charge/discharge process, leading to excellent electrochemical performances, such as 1000 mA h g^{-1} over 1200 cycles and high silicon loading of ca. 4.2 mA h cm^{-2}. Moreover, this binder system is also effective for the thick silicon/graphite electrodes towards practical application.

1. Introduction

With the rapid development of the modern communication, energy storage and traffic technologies, demands for next generation lithium ion batteries with higher energy density become urgent. Due to its high theoretical capacity (4200 mA h g^{-1}, $Li_{22}Si_5$) and moderate delithiation potential (0.4 V vs Li/Li^+), silicon has attracted enormous attentions as a promising anode material [1]. However, silicon undergoes a tremendous expansion and contraction during the lithiation/delithiation process [2], which leads to a series of problems, such as pulverization of silicon, cracking of the electrode, electronic disconnection and the instability of the solid-electrolyte interphase (SEI) [3,4]. To minimize the volume effects, many strategies have been proposed including use of porous silicon structure [5,6], nanosize silicon [7–9] and Si/C composites [10–14]. In addition to active materials, binder is also a key factor which directly affects the electrochemical performance of silicon-based electrodes [15].

At present, the frequently applied binders for silicon-based anodes are sodium carboxymethyl cellulose (CMC) [16], sodium alginate (SA) [15] and polyacrylic acid (PAA) [17], with which the adhering action mainly arises from hydrogen bonds between silicon oxide layers on the Si surfaces and the polar functional groups of the binders. This weak interaction cannot ensure the long-term cycle performance and high areal capacity. To address this issue, various new binders have been investigated, such as polymerized β-cyclodextrin (β-CDp) [18], synthetic self-healing polymers [19,20], gum Arabic [21], xanthan gum (XG) [22], guar gum(GG) [23,24] and some conductive binders [25–27]. Besides these synthetic or natural binders, significant advancements have also been made on ameliorating the existing binders. Crosslinking can enhance the mechanical properties of binders and has been proven to be effective in the binder design [28–32]. It was reported that in-situ crosslinking of PAA with polyvinyl alcohol (PVA) [30] or CMC [29] significantly enhanced the cycle performance of the Si-based anodes. Moreover, in view of that the electrode is an integrated system, binder design from the components interaction and 3-dimensional configuration is important [33].

Here we introduce a coupling agent 3-amino-propyltriethoxysilane (APTES) to Si electrodes, which not only connects Si and PAA covalently but also crosslinks PAA as illustrated in Fig. 1. This 3-dimensional integration strategy enables a high areal capacity (ca. 4.2 mA h cm^{-2}) for silicon electrode with only 10% PAA. Moreover, when applied in thick silicon/graphite electrode for practical consideration, the proposed electrode has exhibited relatively stable cycling behavior over 150 cycles, in comparison with a rapid degradation after the initial several cycles for the conventional Si + PAA electrode.

* Corresponding author.
E-mail address: yangj723@sjtu.edu.cn (J. Yang).

http://dx.doi.org/10.1016/j.electacta.2016.06.152
0013-4686/

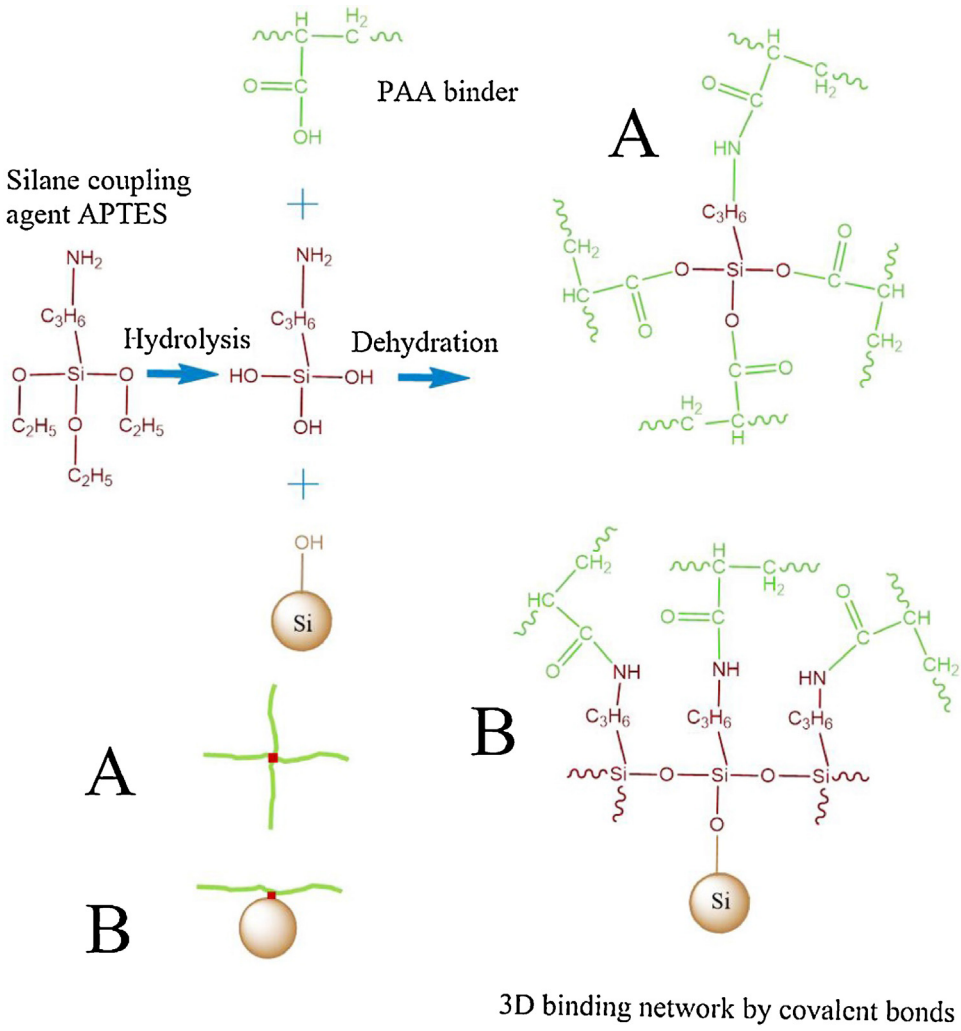

Fig. 1. Design and structure of the electrode with APTES.

2. Experimental

2.1. Electrode preparation

Silicon nanoparticles (50–200 nm, Alfa-Aesar) were mixed with Super P (40 nm, Timical) and PAA (Mv ~ 450 000, Aldrich) in an 8:1:1 weight ratio in water. After stirred for 1 h, a certain amount of APTES (Sinopharm Chemical Reagent Co.) was added and the slurry was stirred for another 4 h. The obtained slurry was coated on a Cu foil current collector and then dried at 70 °C under vacuum for 6 h. Finally, the coated foil was cut to Φ12 mm sheets for assembling cells. Conventional Si + PAA electrode was prepared in the same route just without APTES.

For the thick Si/graphite electrode towards practical application, silicon nanoparticles, nanosized graphite (Timical), KS–6 L (Timical), Super P and PAA were blended in the weight ratio of 40:25:15:5:15 in water. The slurry was stirred for 1 h and then 0.3 wt. % APTES (based on all the electrode materials) was added. The rest routes are the same as the mentioned above.

2.2. Cells assembling and electrochemical tests

The electrochemical performance of the as-prepared anodes was tested via CR2016 coin cells using ENTEK ET20-26 as separator, 1 M $LiPF_6$/EC + DMC (1:1 by volume, ethylene carbonate (EC), dimethyl carbonate (DMC)) as electrolyte, plus 10% fluoroethylene carbonate (FEC), and pure lithium foil as counter electrode. The cells were assembled in an argon-filled glove box (MB-10 compact, MBraun) containing less than 5 ppm water or oxygen. The cycling performance was evaluated on a LAND battery test system (Wuhan Kingnuo Electronics Co., Ltd., China) with constant current densities and the cut-off voltage of 0.01/1.2 V vs Li/Li^+ at 25 °C. The specific capacities were calculated on the basis of the Si weight for silicon anodes and the total weight of all the electrode materials for Si/graphite anodes.

2.3. Morphology and structure characterization

The morphologies and microstructures of the electrodes were observed by a FEI Nova SEM 230 ultra-high resolution FESEM. The Fourier transform infrared (FTIR) spectra of the samples were recorded on a FTIR spectrometer (Bruker VECTOR22), where PAA and APTES were mixed in weight ratio of 1:3 in water, and then dried at 70 °C in vacuum for 6 h while PAA and APTES were directly used for a comparison. For X-ray photoelectron spectroscopy (XPS) tests, 0.5 g silicon nanoparticles and 0.015 g APTES were dispersed in 25 ml water and then stirred for 5 h. Then silicon particles coated by APTES were collected by centrifugation and washed by water. The particles were dried at 70 °C in vacuum for 6 h and designated as Si@APTES. Silicon particles and electrode with 1% APTES were

directly used for a comparison. The XPS analysis was performed using a Kratos Axis UltraDLD spectrometer (Kratos Analytical-A Shimadzu Group Company) with monochromatic Al Kα source (1486.6 eV). Si@APTES and silicon nanoparticles were also used for FTIR tests.

The retained PAA binder on Si particles before and after water washing was estimated by thermogravimetric analysis (TGA, TA 2050). For the sample preparation, silicon particles and PAA were mixed in weight ratio of 2:3 in water. The slurry was stirred for 1 h, and then 1% wt. APTES was added. After stirred for another 4 h, the homogeneous slurry was dried at 70 °C in vacuum for 6 h. Half of the sample was collected for TGA analysis before washing. The other half was vigorously stirred in deionized water for 2 h, and then collected by centrifugation and washed by water for 3 times. The blend was dried at 70 °C in vacuum for 6 h for TGA test. The remaining amounts of PAA were calculated from the mass losses of the blends in TGA tests. The sample without APTES was compared. To evaluate the binder strength, an electrode sample in 20 mm width and 100 mm length was attached to 3 M tape (12 mm wide), and the peel strength of the electrode specimens was measured with a high-precision micromechanical test system (FMT-310A5, Alluris).

3. Results and discussion

3.1. Structure analysis

To verify the reaction of carboxyl in PAA and amino groups in APTES shown in Fig. 1, FTIR spectra of PAA, APTES and PAA + APTES were measured (Fig. 2(a)). For the spectrum of PAA, a peak at 1720 cm^{-1} is attributed to the carbonyl in carboxyl and another at 1457 cm^{-1} to hydroxyl in carboxyl. After mixed with APTES, the peak of hydroxyl almost disappears, and the peak of carbonyl shifts right due to the reaction of carboxyl and amino groups. Moreover, the peak of 1536 cm^{-1} corresponding to amide can be observed, further confirming their reaction. It should be mentioned that PAA + APTES sample after drying at 150 °C in vacuum shows a similar FTIR response to that after drying at 70 °C (Fig. S1 (a)). It means that the crosslinking between APTES and PAA has been completed at 70 °C. To further investigate the structure transformation of PAA after the addition of APTES, TGA and DSC tests were also conducted on PAA and PAA + APTES. Fig. S2 (a) shows that the glass transition temperature (Tg) of PAA is 143 °C while PAA + APTES shows no distinct glass transition during 27 ~ 290 °C. Moreover, the TGA curve of PAA + APTES differs from that of PAA as shown in Fig. S2 (b). These results confirm the crosslinking reaction between PAA and APTES. It was reported that silicon oxide surface on silicon nanoparticles can react with APTES [34–37]. Also, a reaction occurs between APTES and Si, and the modified Si surface contains amino groups, which is verified by the peak corresponding to —NH_2 in N 1 s region of Si@APTES (Fig. 2(b)). Moreover, FTIR spectra of Si@APTES and Si are shown in Fig. S1 (b). The broad band ranging from 3700 to 3200 cm^{-1} is related to the stretching mode of —OH in Si—OH groups, while the two peaks at 3300 cm^{-1} and 3290 cm^{-1} are associated with the asymmetric and symmetric stretching modes of NH_2 in Si@APTES, respectively. The peak at 1641 cm^{-1} corresponds to —OH, and the peaks at 1562 cm^{-1} and 1484 cm^{-1} are assigned to the NH_2 deformation in Si@APTES [38]. These results suggest that APTES was successfully deposited onthe Si surface.

Fig. 3 shows high-resolution XPS spectra of O 1 s regions of Si, Si@APTES and electrode with 1% APTES. The spectra of both Si and Si@APTES can be divided into two peaks corresponding to Si-O-Si and Si-O-H. In fact, silicon nanoparticles are active and easy to form an oxide layer in air, resulting in Si-O-Si and Si-O-H bonds on Si. By comparison, intensity of the peak relating to Si-O-Si in Si@APTES is much greater than that in Si, reconfirming that Si has reacted with APTES to form chemical bonds as shown in situation B in Fig. 1. The spectra of the electrode with 1% APTES in Fig. 3(c) are composed of C—O—Si, Si—O—Si, C=O and C—O—H. The corresponding peak assignments are shown in Fig. 3(d). The C=O bonds and C-O-H bonds should be assigned to PAA in the electrode. The existence of C—O—Si bonds indicates that silicon hydroxyl in APTES reacts with carboxyl in PAA as shown in situation A in Fig. 1. These results reveal that APTES in the electrode possesses dual functions, improving the connections between Si and PAA and crosslinking PAA.

TGA profiles of Si/binder blends after the same washing step have been used to estimate the remaining amount of binder and

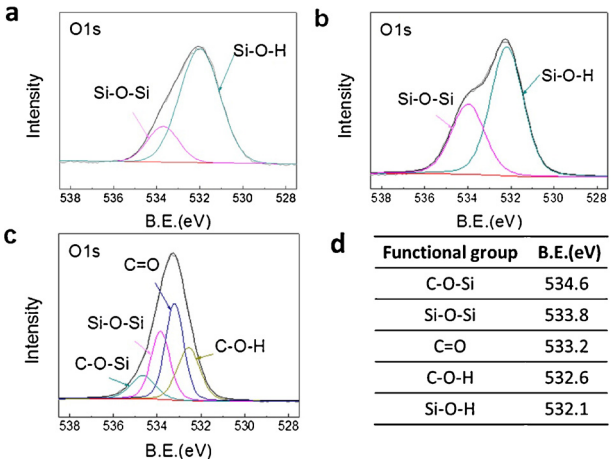

Functional group	B.E.(eV)
C-O-Si	534.6
Si-O-Si	533.8
C=O	533.2
C-O-H	532.6
Si-O-H	532.1

Fig. 3. High-resolution XPS spectra of O 1 s regions of Si (a), Si@APTES (b) and electrode with 1% APTES (c), and the Binding Energy Assignments (d).

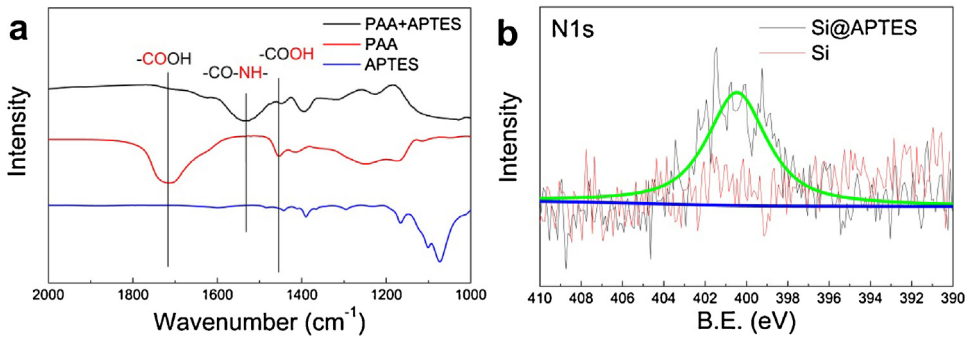

Fig. 2. (a) FTIR spectra of PAA, APTES and PAA + APTES. (b) High-resolution XPS spectra of N 1 s regions of Si and Si@APTES.

binding strength [39,23]. The test results reveal that the remaining amounts of PAA binder with and without APTES are 17.3% and 10.9% of the original amounts after washing the Si/binder blends with water (Table S1). The larger remaining amount of binder after washing means the stronger connection between silicon and binder after the addition of APTES. Moreover, the peeling tests [22,39,40] were also conducted to evaluate the adhesion of the binders. As shown in Fig. S3, the amount of electrode material attached on the tape decreased significantly after the addition of APTES and the peeling force for conventional Si + PAA electrode and the electrode with 0.5% APTES are 0.656 N and 4.968 N, respectively. The multi-linkages of APTES assemble silicon and binder into an entire 3D binding network, leading to higher electrode structure stability during cycling as illustrated in Fig. 4.

3.2. Electrochemical performance

Fig. 5(a) shows the cycling performance and coulombic efficiencies of electrodes with certain amounts of APTES in comparison with the conventional Si + PAA electrode. For the high Si loading electrodes (80%), obvious capacity fluctuation is observable in the initial 20 cycles, which may be caused by multiple factors such as SEI film formation, electrode structure evolution arising from the strong volume changes, and ion transfer limitation at a large current rate of 1.5 A g^{-1}. After 20 cycles, the electrode activation finishes and the capacity fluctuation decreases. Although the electrode without APTES exhibits the initial capacity as high as 3609.4 mA h g^{-1}, it shows poor cycle performance and only ca. 800 mA h g^{-1} is retained after 200 cycles. In contrast, all the electrodes with APTES deliver relatively larger capacities of more than 1600 mA h g^{-1} after 200 cycles. The significant improvement should be attributed to the stronger connection between silicon and binder and the crosslinking structure. Beyond that, the content of APTES also influences the electrochemical performance of the electrodes. The electrode with 0.1 wt.% APTES (based on the mass of silicon) exhibits a capacity of 1871.8 mA h g^{-1} after 200 cycles, compared to 1647.5 mA h g^{-1} for that with 1 wt.% APTES. The higher APTES content corresponds to more crosslinking and hardness. Since the volume change of silicon is unavoidable during the charge/discharge process, too hard and brittle structure cannot endure the volume change and is disadvantageous for cycling [41]. The electrode with 0.5 wt. % APTES cycles most stably after activation and delivers more than 1800 mA h g^{-1} after 200 cycles. This result indicates that a proper connection between silicon and binder and an appropriate degree of binder crosslinking towards a balance between flexibility and hardness are very important for improving the mechanical stability and cycle performance of silicon anode.

To test the long-term cycle performance, the electrodes are tested with a fixed Li insertion capacity of 1000 mA h g^{-1} at 4 A g^{-1} (Fig. 5(b)). The electrode without APTES can only maintain this capacity for less than 500 cycles while electrode with APTES can cycle validly for more than 1200 times, which is much better than the reported results [21,23]. For practical consideration, the silicon loading is increased from 0.5 ~ 0.6 mg cm^{-2} to 2.0 ~ 2.1 mg cm^{-2} with the same electrode composition. As shown in Fig. 5(c), the electrode using only PAA binder displays the reversible capacity of 2802.8 mA h g^{-1} at the first cycle with a low coulombic efficiency (68.3%). However, a much higher capacity of 3174.1 mA h g^{-1} is achieved for the electrode with APTES, corresponding to the initial coulombic efficiency of 76.6%. Furthermore, a comparison of the charge and discharge curves in Fig. 6 reveals that the more serious voltage polarization for the 30th cycle is associated with the electrode without APTES. Due to the dramatic volume change under the extreme conditions of both high mass loading and high Si content, PAA binder is unable to stabilize the electrode structure even at the initial cycle, leading to the partial deactivation and poor electrochemical performance. After the addition of APTES, chemical bonding of silicon and crosslinked PAA reinforce the electrode stability against volume changes during cycling as illustrated in Fig. 4(b). As a result, the cycle performance is significantly improved. After 30 cycles, more than 2100 mA h g^{-1} is maintained, corresponding to ca. 4.2 mA h cm^{-2}, in comparison with less than 1200 mA h g^{-1} for linear PAA binder.

The APTES function is further evaluated for a more practical silicon-graphite electrode in which silicon and graphite are blended in a mass ratio of 8:5 and a total mass loading of 2.0 ~ 2.1 mg cm^{-2}. As shown in Fig. 5(d), the capacity of the electrode without APTES drops sharply in the first few cycles and less than 300 mA h g^{-1} remains after 150 cycles. In contrast, a capacity of 1009.7 mA h g^{-1} is retained for the electrode with APTES, which is also much better than the reported result [22]. The great performance improvement for the thick composite electrode by means of a simple addition of APTES is practically significant.

Fig. 7 shows SEM images of electrodes after 200 cycles at 1.5 A g^{-1}. Distinct cracks of ca. 2 μm on the conventional electrode indicate that linear PAA binder and hydrogen bonds between silicon and binder are unable to accommodate the repeated Si

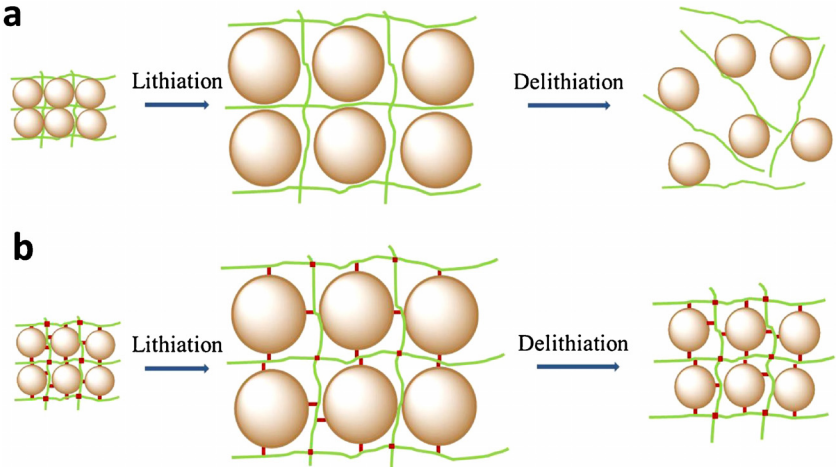

Fig. 4. The possible physical evolution in the lithiation/delithiation process for conventional electrodes (a) and electrodes with APTES (b). The particle break is not in consideration.

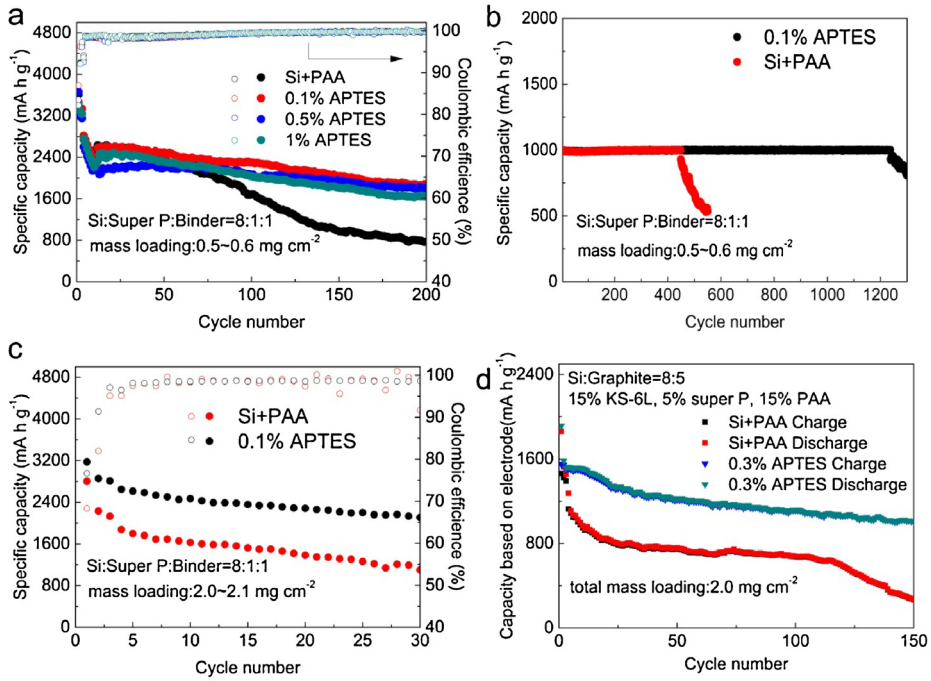

Fig. 5. The cycling performance of electrodes with a certain amount of APTES (the rations are based on the amount of silicon) in comparison with the conventional electrode. (a) Current density: 0.1 A g^{-1} for the first cycle, 0.3 A g^{-1} in the next two cycles and 1.5 A g^{-1} for the rest cycles. (b) The Li insertion capacity was fixed to 1000 mA h g^{-1} Si at 4 A g^{-1} over the potential window of 0.01-1.2 V (versus Li/Li^+). (c) Current density: 0.1 A g^{-1} for the first cycle, 0.3 A g^{-1} in the next two cycles and 0.5 A g^{-1} for the rest cycles. (d) Current density: 0.1 A g^{-1} for the first three cycles, 0.5 A g^{-1} for discharge and 1 A g^{-1} for charge in the following cycles.

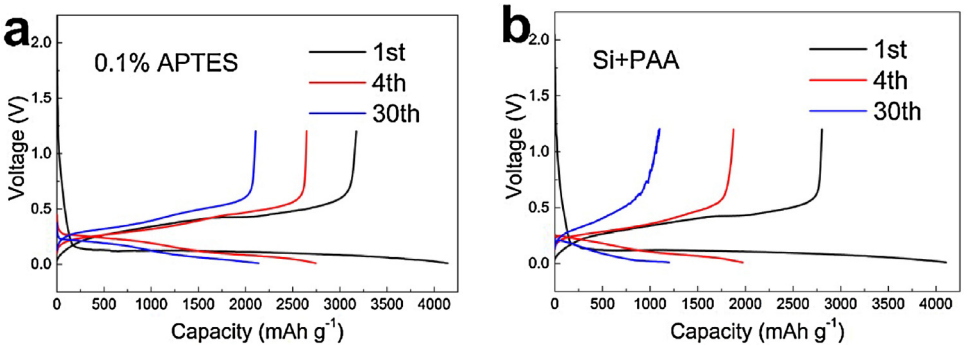

Fig. 6. The charge and discharge curves of electrode with 0.1% APTES (a) and conventional Si + PAA electrode (b) with 2.0 ~ 2.1 mg cm^{-2} material loading.

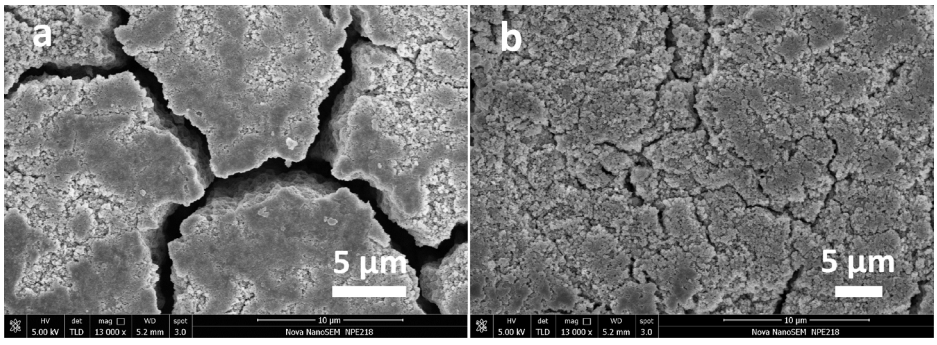

Fig. 7. SEM images of conventional electrode (a, b) and electrode with 0.1% APTES (c, d) after 200 cycles at 1.5 A g^{-1}.

expansion and extraction during cycling, which results in poor cycle performance in Fig. 5(a). After the addition of 0.1% APTES in the slurry, the newly formed chemical interactions can endure the stress caused by the volume change. Thus, the dimensional stability is greatly improved and only slight crevices can be observed.

4. Conclusions

A unique binding strategy for fabrication of silicon based electrodes has been proposed via the addition of APTES to PAA binder, which has the ability of crosslinking PAA along with developing covalent connections between Si and PAA. A proper amount of APTES reinforces electrode stability against the volume change of Si nanoparticles during cycling and significantly enhances the electrochemical performance. The silicon electrodes with 0.1% APTES can cycle for more than 1200 cycles with a fixed Li insertion capacity of 1000 mA h g^{-1} and achieve a high areal capacity of ca. 4.2 mA h cm^{-2} with only 10% of binder. Furthermore, APTES additive is effective for a thick silicon/graphite electrode towards practical application. A capacity of more than 1000 mA h g^{-1} can be retained after 150 cycles, compared to less than 400 mA h g^{-1} for the electrode without APTES. This simple and practical APTES approach facilitates the application of Si based electrodes for high energy Li-ion batteries.

Acknowledgement

This work was supported by State Key Basic Research Program of China (no. 2014CB932303) and SJTU-UM Joint Research Project.

Appendix A. Supplementary data

Supplementary data associated with this article can be found, in the online version, at http://dx.doi.org/10.1016/j.electacta.2016.06.152.

References

[1] R.B. Cervera, N. Suzuki, T. Ohnishi, M. Osada, K. Mitsuishi, T. Kambara, K. Takada, Energ Environ Sci 7 (2014) 662–666.
[2] S.W. Lee, M.T. McDowell, J.W. Choi, Y. Cui, Nano Lett 11 (2011) 3034–3039.
[3] S.F. Lux, I.T. Lucas, E. Pollak, S. Passerini, M. Winter, R. Kostecki, Electrochem Commun 14 (2012) 47–50.
[4] X.H. Liu, H. Zheng, L. Zhong, S. Huan, K. Karki, L.Q. Zhang, Y. Liu, A. Kushima, W. T. Liang, J.W. Wang, J.H. Cho, E. Epstein, S.A. Dayeh, S.T. Picraux, T. Zhu, J. Li, J.P. Sullivan, J. Cumings, C.S. Wang, S.X. Mao, Z.Z. Ye, S.L. Zhang, J.Y. Huang, Nano Lett 11 (2011) 3312–3318.
[5] X. Feng, J. Yang, Y. Bie, J. Wang, Y. Nuli, W. Lu, Nanoscale 6 (2014) 12532–12539.
[6] X. Li, P. Yan, B.W. Arey, W. Luo, X. Ji, C. Wang, J. Liu, J.-G. Zhang, Nano Energy 20 (2016) 68–75.
[7] H.X. Chen, Y. Xiao, L. Wang, Y. Yang, J Power Sources 196 (2011) 6657–6662.
[8] H. Kim, M. Seo, M.H. Park, J. Cho, Angew Chem Int Edit 49 (2010) 2146–2149.
[9] M.A. Rahman, G. Song, A.I. Bhatt, Y.C. Wong, C. Wen, Adv Funct Mater 26 (2016) 647–678.
[10] J.L. Yu, J. Yang, X.J. Feng, H. Jia, J.L. Wang, W. Lu, Ind Eng Chem Res 53 (2014) 12697–12704.
[11] N. Liu, Z.D. Lu, J. Zhao, M.T. McDowell, H.W. Lee, W.T. Zhao, Y. Cui, Nat Nanotechnol 9 (2014) 187–192.
[12] B. Wang, X.L. Li, B. Luo, X.F. Zhang, Y.Y. Shang, A.Y. Cao, L.J. Zhi, Acs Appl Mater Inter 5 (2013) 6467–6472.
[13] Y.T. Bie, J.L. Yu, J. Yang, W. Lu, Y.N. Nuli, J.L. Wang, Electrochim Acta 178 (2015) 65–73.
[14] L. Zhang, R. Rajagopalan, H. Guo, X. Hu, S. Dou, H. Liu, Adv Funct Mater 26 (2016) 440–446.
[15] I. Kovalenko, B. Zdyrko, A. Magasinski, B. Hertzberg, Z. Milicev, R. Burtovyy, I. Luzinov, G. Yushin, Science 334 (2011) 75–79.
[16] H. Buqa, M. Holzapfel, F. Krumeich, C. Veit, P. Novák, J Power Sources 161 (2006) 617–622.
[17] A. Magasinski, B. Zdyrko, I. Kovalenko, B. Hertzberg, R. Burtovyy, C.F. Huebner, T.F. Fuller, I. Luzinov, G. Yushin, Acs Appl Mater Inter 2 (2010) 3004–3010.
[18] M.S. Park, E. Park, J. Lee, G. Jeong, K.J. Kim, J.H. Kim, Y.J. Kim, H. Kim, Acs Appl Mater Inter 6 (2014) 9608–9613.
[19] C. Wang, H. Wu, Z. Chen, M.T. McDowell, Y. Cui, Z.A. Bao, Nat Chem 5 (2013) 1042–1048.
[20] Z. Chen, C. Wang, J. Lopez, Z. Lu, Y. Cui, Z. Bao, Adv Energy Mater 5 (2015) n/a–n/a.
[21] M. Ling, Y.N. Xu, H. Zhao, X.X. Gu, J.X. Qiu, S. Li, M.Y. Wu, X.Y. Song, C. Yan, G. Liu, S.Q. Zhang, Nano Energy 12 (2015) 178–185.
[22] Y.K. Jeong, T.W. Kwon, I. Lee, T.S. Kim, A. Coskun, J.W. Choi, Energ Environ Sci 8 (2015) 1224–1230.
[23] J. Liu, Q. Zhang, T. Zhang, J.-T. Li, L. Huang, S.-G. Sun, Adv Funct Mater 25 (2015) 3599–3605.
[24] R. Kuruba, M.K. Datta, K. Damodaran, P.H. Jampani, B. Gattu, P.P. Patel, P.M. Shanthi, S. Damle, P.N. Kumta, J Power Sources 298 (2015) 331–340.
[25] H. Zhao, Y. Wei, R. Qiao, C. Zhu, Z. Zheng, M. Ling, Z. Jia, Y. Bai, Y. Fu, J. Lei, X. Song, V.S. Battaglia, W. Yang, P.B. Messersmith, G. Liu, Nano Lett 15 (2015) 7927–7932.
[26] X.H. Yu, H.Y. Yang, H.W. Meng, Y.L. Sun, J. Zheng, D.Q. Ma, X.H. Xu, Acs Appl Mater Inter 7 (2015) 15961–15967.
[27] S.M. Kim, M.H. Kim, S.Y. Choi, J.G. Lee, J. Jang, J.B. Lee, J.H. Ryu, S.S. Hwang, J.H. Park, K. Shin, Y.G. Kim, S.M. Oh, Energ Environ Sci 8 (2015) 1538–1543.
[28] J. Liu, Q. Zhang, Z.-Y. Wu, J.-H. Wu, J.-T. Li, L. Huang, S.-G. Sun, Chem Commun 50 (2014) 6386.
[29] B. Koo, H. Kim, Y. Cho, K.T. Lee, N.-S. Choi, J. Cho, Angewandte Chemie International Edition 51 (2012) 8762–8767.
[30] J.X. Song, M.J. Zhou, R. Yi, T. Xu, M.L. Gordin, D.H. Tang, Z.X. Yu, M. Regula, D.H. Wang, Adv Funct Mater 24 (2014) 5904–5910.
[31] T.W. Kwon, Y.K. Jeong, E. Deniz, S.Y. AlQaradawi, J.W. Choi, A. Coskun, Acs Nano 9 (2015) 11317–11324.
[32] J. Lopez, Z. Chen, C. Wang, S.C. Andrews, Y. Cui, Z. Bao, ACS Appl Mater Interfaces 8 (2016) 2318–2324.
[33] Y. Bie, J. Yang, X. Liu, J. Wang, Y. Nuli, W. Lu, ACS Appl Mater Interfaces 8 (2016) 2899–2904.
[34] A. Stein, B.J. Melde, R.C. Schroden, Adv Mater 12 (2000) 1403–1419.
[35] S.W. Song, K. Hidajat, S. Kawi, Langmuir 21 (2005) 9568–9575.
[36] J.S. Bridel, T. Azais, M. Morcrette, J.M. Tarascon, D. Larcher, Chem Mater 22 (2010) 1229–1241.
[37] C. Sun, Y.F. Deng, L.N. Wan, X.S. Qin, G.H. Chen, Acs Appl Mater Inter 6 (2014) 11277–11285.
[38] N. Majoul, S. Aouida, B. Bessais, Appl Surf Sci 331 (2015) 388–391.
[39] Y.K. Jeong, T.-w. Kwon, I. Lee, T.-S. Kim, A. Coskun, J.W. Choi, Nano Lett 14 (2014) 864–870.
[40] M.-H. Ryou, J. Kim, I. Lee, S. Kim, Y.K. Jeong, S. Hong, J.H. Ryu, T.-S. Kim, J.-K. Park, H. Lee, J.W. Choi, Adv Mater 25 (2013) 1571–1576.
[41] J.S. Bridel, T. Azaïs, M. Morcrette, J.M. Tarascon, D. Larcher, Chem Mater 22 (2010) 1229–1241.